Comparison of Three Scattering Models for Ultrasound Blood Characterization

Emilie Franceschini, *Member, IEEE*, Ratan K. Saha, and Guy Cloutier, *Senior Member, IEEE*

***Abstract*—Ultrasonic backscattered signals from blood contain frequency-dependent information that can be used to obtain quantitative parameters reflecting the aggregation level of red blood cells (RBCs). The approach is based on estimating structural aggregate parameters by fitting the spectrum of the backscattered radio-frequency echoes from blood to an estimated spectrum considering a theoretical scattering model. In this study, three scattering models were examined: a new implementation of the Gaussian model (GM), the structure factor size estimator (SFSE), and the new effective medium theory combined with the structure factor model (EMTSFM). The accuracy of the three scattering models in determining mean aggregate size and compactness was compared by 2-D and 3-D computer simulations in which RBC structural parameters were controlled. Two clustering conditions were studied: 1) the aggregate size varied and the aggregate compactness was fixed in both 2-D and 3-D cases, and 2) the aggregate size was fixed and the aggregate compactness varied in the 2-D case. For both clustering conditions, the EMTSFM was found to be more suitable than GM and SFSE for characterizing RBC aggregation.**

I. Introduction

Quantitative ultrasound (US) techniques are mainly based on the frequency analysis of backscattered signals by biological tissues to determine physical properties of the average tissue microstructure. These techniques rely on theoretical scattering models to fit the spectrum of backscattered echoes to an estimated spectrum using an appropriate model. The theoretical scattering model most frequently used for this purpose is the Gaussian model (GM) [1], [2], which yields two tissue properties: the average scatterer size and the acoustic concentration (i.e., the product of the scatterer number density by the square of the relative impedance difference between scatterers and the surrounding medium). This approach has been used to characterize dilute scattering media such as the eye [3], prostate [4], and breast [5]. Blood has also been studied with this technique [6], although estimations could be biased.

Manuscript received May 22, 2013; accepted August 7, 2013. This work was supported by the Fonds Incitatifs Recherche of the Université de Provence and by an operating grant from the Canadian Institutes of Health Research (grant number MOP-84358).

E. Franceschini is with the Laboratoire de Mécanique et d'Acoustique (LMA), CNRS UPR 7051, Aix-Marseille University, Marseille, France (e-mail: franceschini@lma.cnrs-mrs.fr).

R. K. Saha is with the Saha Institute of Nuclear Physics, Applied Material Science Division, Bidhannagar, Kolkata, India.

G. Cloutier is with the Laboratory of Biorheology and Medical Ultrasonics, University of Montreal Hospital Research Centre (CRCHUM), Montreal, QC, Canada, and with the Department of Radiology, Radio-Oncology and Nuclear Medicine, and Institute of Biomedical Engineering, University of Montreal, Montreal, QC, Canada (e-mail: guy.cloutier@umontreal.ca).

DOI http://dx.doi.org/10.1109/TUFFC.2013.2829

An important contribution of ultrasonic blood characterization is to assess the level of red blood cell (RBC) aggregation, which is a surrogate marker of inflammation [7]. It is well known that when RBCs are under low shear rates ($<10\ s^{-1}$), they interact strongly with each other and form complex rouleaux or 3-D structures. When the shear rate increases, these rouleaux or compact structures disaggregate. This aggregation phenomenon is normal in human blood, however hyperaggregation is a pathological state associated with several circulatory diseases, such as deep venous thrombosis, atherosclerosis, and diabetes mellitus. Blood characterization using US backscatter techniques provides a unique opportunity to monitor RBC aggregation noninvasively and *in vivo* within blood vessels. This quantification may help to elucidate the role of RBC aggregation in the etiology of such diseases.

US backscatter by blood is mainly due to RBCs that constitute the vast majority (97%) of the blood cellular content. Blood can thus be described as a biphasic fluid composed of RBCs immersed in plasma. Because RBCs are acoustically considered as weak scatterers (impedance contrast between RBCs and plasma being around 13%), multiple scattering can be neglected. However, for such tissue, it is not straightforward to develop a theoretical scattering model because of the high density of RBCs (their volume fraction or hematocrit varies between 30% and 50%) and their ability to form aggregates. The structure factor model (SFM) [8], [9] is a US scattering model proposed to simulate the backscatter coefficient (BSC) of aggregated RBCs. The SFM sums the acoustic contributions from individual RBCs and models their interaction by a statistical mechanics structure factor, which is by definition the Fourier transform of the spatial distribution of RBCs [8], [9]. However, the SFM can hardly be implemented to estimate the structural aggregate parameters in the framework of an inverse problem formulation because of the intensive computational time required to assess the structure factor with distributions of aggregating RBCs. That is why Yu and Cloutier [10] developed the structure factor size estimator (SFSE) scattering theory, which approximates the SFM by using a second-order Taylor expansion of the structure factor. The SFSE is thus not as accurate as the SFM. The SFSE estimates two physical parameters describing the microstructure of RBC aggregates: the packing factor, which increases with erythrocyte clustering, and the average aggregate isotropic radius. However, experiments with pig blood in controlled flow devices [10] and 3-D numerical simulations of isotropic monodisperse aggregates [11] recently showed that the two indices are correlated and follow a quadratic

relationship, thus reducing the BSC parameterization to one structural index.

A scattering model called the effective medium theory combined with the SFM (EMTSFM) was recently proposed to better approximate the SFM [12]. It assumes that aggregates of RBCs can be treated as individual homogeneous scatterers which have effective properties determined by the acoustical characteristics and concentration of RBCs within aggregates. The EMTSFM allows characterization of the radius, and for the first time in the quantitative US field, the compactness of RBC aggregates [12]. In the field of clinical hemorheology [13], assessing the compactness of RBC aggregates is of high clinical importance because it is related to the binding energy between cells. Normal RBC aggregates form rouleaux-type structures, whereas pathologies associated with stronger binding energies result in clumps of RBCs (close to a spherical isotropic packing) [14], [15].

In our previous study [12], the EMTSFM and the SFM were compared in the framework of a forward-problem study to determine the BSC from a known distribution of RBCs with known acoustical parameters. The goodness of the approximation of the EMTSFM in comparison with the SFM was examined as a function of frequency and structural aggregate parameters (aggregate size and compactness). Based on a 2-D simulation study, the EMTSFM was found to approximate the SFM with relative errors less than 30% for a product of the wavenumber times the mean aggregate radius $kr_{\mathrm{ag}} \leq 1.32$ [12]. The goals of the present paper are:

- to evaluate the EMTSFM in an inverse-problem framework, i.e., to determine RBC structural features from the measured BSC, and
- to compare the EMTSFM with two other scattering models: the SFSE and a new implementation of the GM slightly modified to treat aggregating scatterers.

To our knowledge, there is no means to experimentally assess aggregate sizes at a normal physiological hematocrit of 40% because RBCs at that hematocrit are opaque to light. It would thus not be feasible to quantitatively evaluate the performance of the different models with real experimental data. In the field of blood imaging and characterization, the assessment of accuracy of a scattering model was only performed at a low hematocrit of 6% by comparing optical and acoustic measurements of RBC aggregate sizes [10]. In the current paper, we thus aim to determine the performance of three theoretical scattering models (the new implementation of the GM, the SFSE, and the EMTSFM) to extract the aggregation parameters from computer simulations where RBC structural parameters (such as the hematocrit, the aggregate size, and compactness) are known.

The important contribution of the EMTSFM is the parameterization of the BSC with the aggregate compactness [12], which is a structural parameter not available in any other modeling strategies proposed in quantitative US. The potential of the EMTSFM and of the two other scattering models in estimating the aggregate compactness was examined by 2-D computer simulations based on the SFM in controlled clustering configurations (when the aggregate compactness varies and the aggregate radius is fixed). This clustering condition was only conducted in 2-D because of the computational load required to generate 3-D RBC distributions with various aggregate compactnesses with the SFM [12]. Some 3-D computer simulations were also used in the same controlled clustering configurations as those used in 2-D (when the aggregate size varies and the aggregate compactness is fixed) to compare the BSC behavior between 2-D and 3-D simulations, and estimated structural aggregate parameters with the three scattering models.

II. Computer Simulations Based on the Structure Factor Model (SFM)

This section presents computer simulations performed to predict the frequency dependence of the BSC from aggregated RBCs based on the SFM. In the following, it is assumed that the incident wavelength λ is large compared with the RBC size. Consequently, the RBC shape could be approximated by a simple geometry having an equivalent surface in 2-D or having an equivalent volume of a RBC in 3-D [16]. RBCs were modeled as parallel infinite cylinders in the 2-D case and as spheres in the 3-D case of radius a, that have small contrast in acoustical properties relatively to the plasma (see Table I). This RBC shape approximation has some limitations for larger frequencies (>20 MHz) and will be discussed later in Section V-C.

The SFM describing US backscatter by biological tissues consists of summing contributions from cells and modeling the cellular interaction by a statistical mechanics structure factor [8], [9]. By considering a collection of N identical and weak scattering RBCs, the BSC expression can be written as

$$\mathrm{BSC}_{\mathrm{SFM}}(-2k) = m\sigma_{\mathrm{b}}(-2k)S(-2k), \tag{1}$$

where k is the wavenumber and m is the number density of RBCs, which is related to the systemic hematocrit ϕ as $m = \phi/A_{\mathrm{p}}$ (where A_{p} is the RBC area) for 2-D modeling, or as $m = \phi/V_{\mathrm{p}}$ (where V_{p} is the RBC volume) for 3-D modeling. The backscattering cross section σ_{b} of a single weak RBC was calculated using the fluid infinite cylinder expression in the 2-D case [12] or using the fluid-filled sphere expression in the 3-D case [17], [18], given by

TABLE I. Acoustical Properties of Blood Found in [16] and [21].

	Density ρ (kg·m^{-3})	Compressibility κ (Pa^{-1})	Impedance Z (MRayl)
RBC	1092	3.41×10^{-10}	1.766
Plasma	1021	4.09×10^{-10}	1.580

$$\sigma_{\mathrm{b}}(-2k) = \frac{k^3 A_{\mathrm{p}}^2 \gamma_z^2}{2\pi}\left(\frac{J_1(2ka)}{ka}\right)^2 \text{ in the 2-D case}$$
$$= \frac{k^4 V_{\mathrm{p}}^2 \gamma_z^2}{4\pi^2} \times \left(3\frac{\sin(2ka) - 2ka\cos(2ka)}{(2ka)^3}\right)^2 \text{ in the 3-D case,} \quad (2)$$

where J_1 is the first-order Bessel function of the first kind and γ_z is the relative impedance difference between the RBC and its suspending medium (i.e., the plasma). The function S is the structure factor representing the spatial positioning of RBCs, and is defined by

$$S(-2k) = E\left[\frac{1}{N}\left|\sum_{i=1}^{N} e^{-i2\boldsymbol{k}\boldsymbol{r}_i}\right|^2\right], \quad (3)$$

where E represents the expected value of a random variable and $\boldsymbol{r}_i$ is the position vector defining the center of the ith RBC in space. In general, the structure factor of a medium containing RBCs distributed in a 2-D space (or in the 3-D space) can be determined from the 2-D Fourier transform (or 3-D Fourier transform) of the spatial distribution of particles (see [19, Appendix]).

The computation of the $\mathrm{BSC_{SFM}}$ using the SFM requires an intensive computation because of the calculation of the structure factor S as described in (1). Because the structure factor is by definition a statistical quantity, an average of structure factors from several RBC spatial distributions can give an estimated value of S. Because of the computational load to generate aggregating RBC distributions, a simple and fast method was used to randomly generate non-overlapping RBC aggregates which were isotropic and similar in size. For the 2-D and 3-D computer simulations, the simulated $\mathrm{BSC_{SFM}}$ were obtained from the method described in [12, Section III] and [11, Section III], respectively. Note that 2-D simulations are computationally less intensive but significant insights can be gained by studying 2-D systems. On the other hand, 3-D simulations are intuitively appealing because they better mimic experimental situations, but are computationally important. These methods are briefly summarized in the following.

Random distributions for aggregating RBCs were computed within the simulated surface area of $600 \times 600\ \mu\mathrm{m}^2$ in the 2-D case and within the simulated volume of $1000 \times 125 \times 125\ \mu\mathrm{m}^3$ in the 3-D case. The RBC radius a was set to 2.75 μm for all simulations. We first specified the systemic hematocrit ϕ, the aggregate radius r_{ag}, and the aggregate compactness ϕ_i (i.e., the RBC concentration within aggregates). Aggregates of identical radii r_{ag} and of identical compactness ϕ_i were then randomly distributed with non-overlapping positions to give the desired concentration of aggregates $\phi_{\mathrm{ag}} = \phi/\phi_i$. Note that in the case of the 3-D study, a small number of non-aggregated RBCs was added to reach the desired systemic hematocrit. This means that all RBCs were aggregated in blood in the 2-D case, whereas in the 3-D case, a fraction of RBCs were aggregated and the rest remained disaggregated. Finally, RBC distributions within aggregates were generated as follows:

- in the 2-D case, the locations of the RBCs were generated using external and repulsive forces to obtain random RBC positions inside each aggregate, such that the distribution of RBCs within each aggregate was different [12]. This technique allowed several aggregation configurations to be studied: 1) the aggregate size varied and the aggregate compactness was fixed to 0.6, and 2) the aggregate compactness varied from 0.3 to 0.6 and the aggregate size was fixed.
- in the 3-D case, the RBCs were stacked by following a hexagonal close packing (HCP) structure for each aggregate, such that the distribution of RBCs within each aggregate was identical. This HCP structure provides the highest compactness, at about 0.74 for spheres [11]. Therefore, this technique allowed several aggregation configurations to be studied in which the aggregate size varied and the aggregate compactness was fixed at 0.74.

For each distribution of RBCs, the 2-D or 3-D Fourier transformation of the spatial organization of RBCs was then computed to obtain the corresponding structure factor. A mean structure factor was determined from 400 different tissue realizations in the 2-D case (see [12, Section III-B]) and from 250 different tissue realizations in the 3-D case (see [11, Section III-B]).

III. Ultrasound Backscattering Modeling for the Estimation of Structural Aggregate Parameters

As seen in Section II, the SFM allows simulation of the BSC from RBCs whatever the RBC spatial distribution (i.e., disaggregated or aggregated RBCs and/or with various aggregate sizes and compactnesses). However, the SFM can hardly be implemented to estimate structural parameters in the framework of an inverse problem formulation because of the intensive computational time to assess the structure factor by realizing distributions of RBCs with simulations. That is why two scattering theories, named the SFSE and the EMTSFM, have recently been developed to approximate the SFM for practical assessments of RBC structural features (i.e., in an inverse problem formulation). This section presents these two scattering theories (the SFSE and the EMTSFM) as well as the GM also used for tissue characterization. In this work, we present a new implementation of the GM model inspired by our development on EMTSFM. All three theories fit a curve to the simulated $\mathrm{BSC_{SFM}}$ from blood to estimate aggregation parameters using the minimization routine fminsearch in Matlab (The MathWorks Inc., Natick, MA); i.e., a Nelder–Mead simplex method. Note that this fit was realized in

$$\sigma_{\mathrm{ag}}(-2k) = \frac{k^3\pi r_{\mathrm{ag}}^4\gamma_{z_{\mathrm{ag}}}^2}{2}\left(\frac{J_1(2kr_{\mathrm{ag}})}{kr_{\mathrm{ag}}}\right)^2 \text{ in the 2-D case}$$
$$= \frac{4k^4 r_{\mathrm{ag}}^6\gamma_{z_{\mathrm{ag}}}^2}{9}\left(3\frac{\sin(2kr_{\mathrm{ag}}) - 2kr_{\mathrm{ag}}\cos(2kr_{\mathrm{ag}})}{(2kr_{\mathrm{ag}})^3}\right)^2 \text{ in the 3-D case} \quad (8)$$

the frequency bandwidth from 4 MHz to the frequency corresponding to the first minimum of the $\mathrm{BSC_{SFM}}$ (i.e., after the frequency-dependent increase in BSC followed by a peak and a reduction to its first minimum).

A. The Structure Factor Size Estimator (SFSE)

The SFSE developed by Yu and Cloutier [10] approximates the SFM with a second-order Taylor expansion of the structure factor in k as follows:

$$S(-2k) \approx W - 4(kR_{\mathrm{g}}a)^2 \text{ in the 2-D case}$$
$$\approx W - 4(kR_{\mathrm{g}}a)^2 \approx W - \frac{12}{5}(kR_{\mathrm{sp}}a)^2 \text{ in the 3-D case,} \quad (4)$$

where W is the low-frequency limit of the structure factor ($S(k)|_{k\to 0}$), called the packing factor [20], [21], and R_{g} is the radius of gyration of RBC aggregates, assumed to be isotropic and expressed in number of RBCs [10]. Note that in the 3-D case, R_{g} is related to the isotropic radius R_{sp} of an aggregate (expressed in number of RBCs) by $R_{\mathrm{g}} = \sqrt{3/5}R_{\mathrm{sp}}$ [11], [22]. By assuming identical RBCs, and recombining (1) and (4), the SFSE model approximates the BSC as

$$\mathrm{BSC_{SFSE}}(-2k) = \frac{1}{2\pi}mk^3A_{\mathrm{p}}^2\gamma_z^2\left(\frac{J_1(2ka)}{ka}\right)^2$$
$$\times\left(W - 4(kR_{\mathrm{g}}a)^2\right) \text{ in the 2-D case}$$
$$= \frac{1}{4\pi^2}mk^4V_{\mathrm{p}}^2\gamma_z^2\left(3\frac{\sin(2ka) - 2ka\cos(2ka)}{(2ka)^3}\right)^2$$
$$\times\left(W - \frac{12}{5}(kR_{\mathrm{sp}}a)^2\right) \text{ in the 3-D case.} \quad (5)$$

The SFSE assumes that the hematocrit ϕ, the RBC radius a, and the acoustical properties of plasma and RBCs are known *a priori*. Therefore, (5) presents only two unknowns that characterize the aggregate structure: W and R_{g} (or equivalently, W and R_{sp} in the 3-D case). Estimated values of W^* and R_{g}^* (or equivalently, W^* and R_{sp}^* in the 3-D case) were determined by fitting the simulated $\mathrm{BSC_{SFM}}$ given by (1) with $\mathrm{BSC_{SFSE}}$ given by (5).

B. The Effective Medium Theory Combined With the Structure Factor Model (EMTSFM)

The EMTSFM assumes that all the scatterers are aggregated, that the aggregates are identical and isotropic, and that the scatterers within aggregates are evenly distributed [12]. In the case of blood backscatter, the model consists of treating the RBC aggregates as individual homogeneous particles of radius r_{ag}. These homogeneous particles are characterized by a density ρ_{ag} and a compressibility κ_{ag} derived from the acoustical properties of the two fluids constituting them (i.e., ρ_1, ρ_2, κ_1, and κ_2, where 1 indicates properties of RBCs and 2 indicates those of plasma), and from the internal concentration of RBCs within the aggregates, defined as the aggregate compactness ϕ_i, as follows:

$$\rho_{\mathrm{ag}} = \phi_i\rho_1 + (1-\phi_i)\rho_2$$
$$\frac{1}{\kappa_{\mathrm{ag}}} = \frac{\phi_i}{\kappa_1} + \frac{1-\phi_i}{\kappa_2}. \quad (6)$$

The BSC from blood is then obtained by summing contributions from individual effective particles of radius r_{ag} and modeling the effective particle interaction by a statistical mechanics structure factor S_{ag}. The equivalent BSC expression is thus given by [12]

$$\mathrm{BSC_{EMTSFM}}(-2k) = m_{\mathrm{ag}}\sigma_{\mathrm{ag}}(-2k)S_{\mathrm{ag}}(-2k), \quad (7)$$

where S_{ag} is the structure factor of a collection of N_{ag} randomly distributed identical particles of radius r_{ag} and m_{ag} is the number density of aggregates, which is related to the effective aggregate concentration ϕ_{ag}. The effective aggregate concentration is equal to the RBC concentration in blood ϕ divided by the aggregate compactness ϕ_i: $\phi_{\mathrm{ag}} = \phi/\phi_i$. The backscatter cross section of an effective single-particle σ_{ag} was calculated using the fluid infinite cylinder expression in the 2-D case [12] or using the fluid-filled sphere expression in the 3-D case [17], [18] given by (8), see above, where z_{ag} is the impedance of the equivalent particle and $\gamma_{z_{\mathrm{ag}}}$ is the relative impedance difference between the equivalent particle and the plasma ($\gamma_{z_{\mathrm{ag}}} = (z_{\mathrm{ag}} - z_2)/z_2$). For a random distribution of hard cylinders in 2-D, the structure factor was numerically computed as described in Appendix A. For a random distribution of hard spheres in 3-D, the structure factor can be analytically calculated as established by Wertheim [23]. The analytical expression for the structure factor in the 3-D case is described in Appendix B.

By assuming that the hematocrit ϕ, the RBC radius a, and the acoustical properties of plasma and RBCs are known *a priori*, the unknown parameters are the radius of aggregates r_{ag} and their compactness ϕ_i. The unknown

parameters were estimated by matching the simulated $\mathrm{BSC_{SFM}}$ given by (1) with the theoretical $\mathrm{BSC_{EMTSFM}}$ given by (7).

C. The Gaussian Model (GM)

Using the GM, the BSC is modeled with a spatial autocorrelation function describing the shape and distribution of scatterers in the medium. The scattering sites are assumed to be randomly distributed and of simple geometric shapes, represented as Gaussian scatterers mimicking continuous changes in impedance. In this framework, the BSC can be written as the product of the theoretical BSC under Rayleigh scattering and the backscatter form factor (see [18, Eqs. (74)–(76)] for the GM formulation in 3-D). The form factor describes the frequency dependence of BSC attributed to the size and shape of the prototype scatterer. The Gaussian form factor has been used for many applications [3]–[6]. It represents tissue structures as continuously varying distributions of acoustic impedance fluctuations about the mean value, and the effective radius is related to the impedance distribution of the scatterers.

The BSC for the GM formulation is written as the product of the BSC in the Rayleigh limit and the backscatter form factor as [18]

$$\begin{aligned}\mathrm{BSC_{GM}}(-2k) &= \frac{k^3 S_s^2 n_z}{2\pi} e^{-2k^2d^2} \\ &= \frac{\pi k^3 a_{\mathrm{eff}}^4 n_z}{2} e^{-k^2 a_{\mathrm{eff}}^2} \text{ in the 2-D case} \\ &= \frac{k^4 V_s^2 n_z}{4\pi^2} e^{-2k^2d^2} \\ &= \frac{4k^4 a_{\mathrm{eff}}^6 n_z}{9} e^{-0.827k^2 a_{\mathrm{eff}}^2} \text{ in the 3-D case,}\end{aligned} \tag{9}$$

where n_z is the acoustic concentration (i.e., the product of the number density of scatterers times the square of the relative impedance difference γ_z between scatterers and the surrounding tissue). In the 2-D case (or respectively in the 3-D case), the characteristic dimension d is related to the area of the effective scatterer S_s by $S_s = 2\pi d^2$ [or related to the volume of the effective scatterer V_s by $V_s = (2\pi d^2)^{3/2}$]. Continuous isotropic media can be characterized by the correlation distance d, in the same way that discrete isotropic media are characterized by a scatterer radius [18]. The effective radius of the scatterer a_{eff} is related to the correlation distance d by setting values of S_s (or V_s, respectively) for a continuum model equal to the area of an effective cylinder (or equal to the volume of an effective scatterer) of radius a_{eff}: $S_s = 2\pi d^2 = \pi a_{\mathrm{eff}}^2$ or $V_s = (2\pi d^2)^{3/2} = (4/3)\pi a_{\mathrm{eff}}^3$.

Estimates of the effective radius a_{eff}^* and acoustic concentration n_z^* were determined by fitting the simulated $\mathrm{BSC_{SFM}}$ given by (1) with the $\mathrm{BSC_{GM}}$ given by (9). Effective radii a_{eff} estimated with the GM have been hypothesized to be related to the aggregate radii, and the acoustic concentration n_z is postulated to be the product of the number density of aggregates times the square of the relative impedance difference between aggregates and the plasma as follows:

$$\begin{aligned}n_z &= \gamma_{z_{\mathrm{ag}}}^2 \frac{\phi_{\mathrm{ag}}}{\pi a_{\mathrm{eff}}^2} = \left(\frac{z_{\mathrm{ag}} - z_2}{z_2}\right)^2 \frac{\phi}{\phi_i \pi a_{\mathrm{eff}}^2}, \text{ in the 2-D case} \\ &= \gamma_{z_{\mathrm{ag}}}^2 \frac{3\phi_{\mathrm{ag}}}{4\pi a_{\mathrm{eff}}^3} = \left(\frac{z_{\mathrm{ag}} - z_2}{z_2}\right)^2 \frac{3\phi}{4\phi_i \pi a_{\mathrm{eff}}^3}, \text{ in the 3-D case,}\end{aligned} \tag{10}$$

where z_{ag} is the effective impedance of the aggregates approximated by the mixing law: $z_{\mathrm{ag}} = \phi_i z_1 + (1 + \phi_i) z_2$. Because the hematocrit ϕ and the acoustical properties of plasma and RBCs are assumed to be known *a priori*, the aggregate compactness can be deduced from the estimated parameters a_{eff}^* and n_z^* by using (10) as follows:

$$\begin{aligned}\phi_i^* &= \frac{\pi {a_{\mathrm{eff}}^*}^2 n_z^* z_2^2}{\phi(z_2 - z_1)^2} \text{ in the 2-D case} \\ &= \frac{4\pi {a_{\mathrm{eff}}^*}^3 n_z^* z_2^2}{3\phi(z_2 - z_1)^2} \text{ in the 3-D case.}\end{aligned} \tag{11}$$

This means that the new proposition of the GM was employed in our study as an effective medium model, but unlike the EMTSFM, the GM is not combined with the SFM (such that the GM is assumed to be accurate only at low systemic hematocrits). In the following, we thus give the estimated parameters a_{eff}^* and ϕ_i^* with the GM, instead of the classical estimated parameters a_{eff}^* and n_z^*.

IV. Results

This section gives the results of the inverse problem obtained for 2-D and 3-D computer simulations with the three aforementioned backscattering models: SFSE, EMTSFM, and GM.

A. Results Obtained From the 2-D Computer Simulations

For the 2-D computer simulations, we first studied clustering configurations in which the aggregate compactness was fixed to $\phi_i = 60\%$ and the aggregate radius r_{ag}/a varied, and then clustering configurations in which the aggregate radius was fixed to $r_{\mathrm{ag}}/a = 6.32$ and the aggregate compactness ϕ_i varied.

1) Results for the SFSE: The SFSE was first examined for systemic hematocrits of 10%, 20%, and 30% when the aggregate size varied and the aggregate compactness was fixed to a high value: $\phi_i = 60\%$. Fig. 1 shows $\mathrm{BSC_{SFM}}$ as a function of frequency for different aggregate sizes and systemic hematocrits. The symbols represent the $\mathrm{BSC_{SFM}}$ computation for the disaggregated case ($r_{\mathrm{ag}}/a = 1$) and for aggregation with radii $r_{\mathrm{ag}}/a = 3.16$, 5.0 and 7.07. Also represented by dashed lines in Fig. 1 are the corresponding $\mathrm{BSC_{SFSE}}$ fitted curves. The first peaks of the simulated

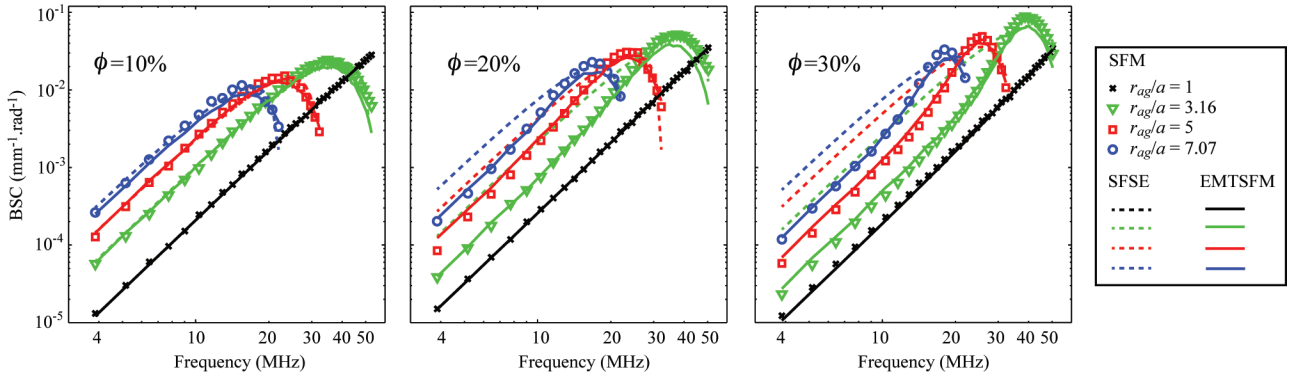

Fig. 1. Frequency-dependent backscatter coefficients (BSCs) for different aggregate sizes and a constant aggregate compactness $\phi_i = 60\%$ at systemic hematocrits of 10%, 20%, and 30%. The symbols represent the BSC_{SFM} computation. The dashed lines represents the corresponding fitting with the SFSE, whereas the solid lines expresses the fitting with the EMTSFM.

BSC_{SFM} occur at lower frequencies as the aggregate radius increases. Because the fitting curves with the SFSE were realized in the frequency bandwidth from 4 MHz to the frequency corresponding to the first minimum of the BSC_{SFM} (except for the disaggregated case, for which the frequency bandwidth is from 4 to 50 MHz), the bandwidth used for the fitting becomes smaller as the aggregate radius increases. It is clear from the figure that the SFSE provided better fits for the lower hematocrit of 10%. As the hematocrit increases, the SFSE model is insufficient to predict the behavior of BSC_{SFM}, especially in the low-frequency range. The estimated values of W^* and R_g^* are given in Table II for systemic hematocrits of 10%, 20%, and 30%. In this table, the relative error for parameter R_g^* corresponds to: $\varepsilon_{R_g^*} = (R_g^* - (r_{ag}/a))/(r_{ag}/a)$. Fig. 2(a) shows the estimated values of R_g^* as a function of the actual aggregate radii r_{ag}/a for all hematocrits. Also represented are the corresponding linear regression lines showing good correlation $r^2 \geq 0.95$ at all hematocrits. For radii r_{ag}/a between 4.47 and 7.95, relative errors $\varepsilon_{R_g^*}$ were less than 30% for hematocrits of 10% and 20%. It is interesting to notice that estimated parameters W^* and R_g^* follow a linear relation for all hematocrits [see Fig. 2(b)].

The SFSE was also evaluated at systemic hematocrits of 10% and 20% when the aggregate size r_{ag}/a was fixed at 6.32 and the aggregate compactness ϕ_i varied from 30% to 60%. It is important to emphasize that 2-D random particle distributions could be easily generated using a random number generator up to an area fraction of approximately 0.5. For the 20% systemic hematocrit, aggregate compactnesses smaller than 40% could not be computed because the corresponding area fractions of aggregates were too high: $\phi_{ag} > 0.5$. Similarly, the variation of the aggregate compactness could not be performed at a systemic hematocrit of 30% because the area fractions of aggregates are already equal to 0.5 for an aggregate compactness $\phi_i = 60\%$. Fig. 3 displays BSC_{SFSE} in dashed lines for the following clustering conditions: $r_{ag}/a = 6.32$ and ϕ_i varying from 30% to 60%. One can observe large differences between simulated and fitted SFSE curves, especially at low frequencies where the fitted curves overestimate the BSC_{SFM} amplitude. These differences are larger at $\phi = 20\%$. The estimated values of R_g^* for different aggregate compactnesses are plotted in Fig. 4(a). Although the true radius is fixed, estimated R_g^* increases with the aggregate compactness at both hematocrits. We found no correlation between the actual fixed radius and the estimated radii ($r^2 < 0.06$). Notice the linear relation between W^* and R_g^* when the aggregate compactness varies [see Fig. 4(b)], as observed previously in Fig. 2(b) when the aggregate radius r_{ag}/a was changed.

2) Results for the EMTSFM: The BSC curves fitted with the EMTSFM are shown in solid lines in Fig. 1 for the case of varying values of r_{ag}/a, and in Fig. 3 for varying ϕ_i. In both cases, the EMTSFM provided good fittings to the simulated BSC_{SFM} curves for all systemic hemato-

TABLE II. VALUES OF THE AGGREGATE RADIUS AND COMPACTNESS USED FOR COMPUTATION OF THE SIMULATED BSC_{SFM}, AND VALUES OF PARAMETERS FOUND WITH THE SFSE.

SFM		$\phi = 10\%$			$\phi = 20\%$			$\phi = 30\%$		
r_{ag}/a	ϕ_i (%)	W^*	R_g^*	$\varepsilon_{R_g^*}$ (%)	W^*	R_g^*	$\varepsilon_{R_g^*}$ (%)	W^*	R_g^*	$\varepsilon_{R_g^*}$ (%)
1	100	0.61	0.39	−61.00	0.37	0.39	−61.00	0.17	0.38	−62.00
3.16	60	3.12	1.50	−52.53	3.29	1.56	−50.63	2.67	1.32	−58.23
5	60	7.41	3.81	−23.80	6.95	3.64	−27.20	5.31	3.04	−39.20
7.07	60	15.82	7.99	13.01	13.57	7.18	1.56	8.58	5.33	−24.61

Aggregating conditions: r_{ag}/a varies, ϕ varies, $\phi_i = 60\%$ (except in the case of diaggregated RBCs where $\phi_i = 100\%$). The parameter ε indicates the relative error.

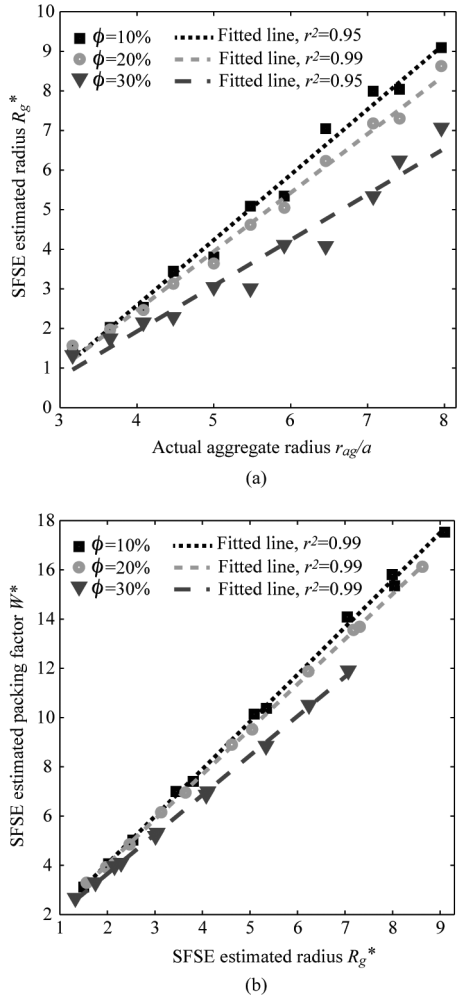

Fig. 2. (a) Comparison of R_g^* estimated with SFSE and the actual aggregate size r_{ag}/a for the three systemic hematocrits 10%, 20%, and 30%. (b) Linear relationships between W^* and R_g^*. Results presented here correspond to the configuration where r_{ag}/a varies and ϕ_i is fixed.

crits. For the clustering conditions in which the aggregate radius varied and the aggregate compactness was constant, the estimated values r_{ag}^*/a and ϕ_i^* and the corresponding relative errors are given in Fig. 5 for systemic hematocrits of 10%, 20%, and 30%. For the clustering conditions in which the aggregate compactness varied and the aggregate radius was constant, the results are shown in Fig. 6 for systemic hematocrits of 10% and 20%. For the EMTSFM, the relative errors for each parameter correspond to

$$\varepsilon_{r_{ag}^*} = \frac{(r_{ag}^*/a) - (r_{ag}/a)}{(r_{ag}/a)} \quad \text{and} \quad \varepsilon_{\phi_i^*} = \frac{\phi_i^* - \phi_i}{\phi_i}. \quad (12)$$

In both sub-studies in which the aggregate radius and compactness varied, a very good correspondence can be observed between true and estimated aggregate sizes and compactnesses. The relative errors for the estimated aggregate radii and compactnesses were less than 13% and 14%, respectively, for all hematocrits and for all studied aggregating configurations.

3) Results for the GM: Fig. 7 presents the $\mathrm{BSC_{SFM}}$ curves fitted with the GM for several aggregate sizes at the same clustering conditions as in Fig. 1. The GM provided overestimations in the low-frequency range for all

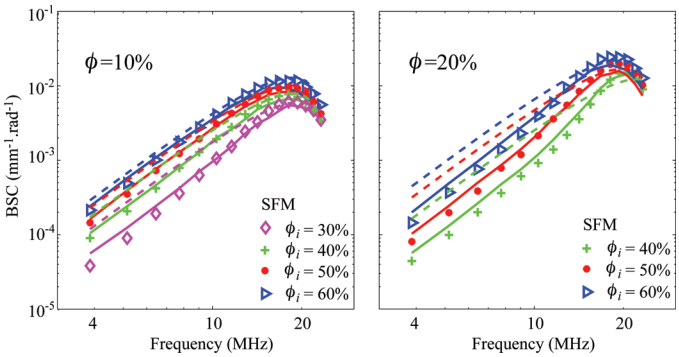

Fig. 3. Frequency-dependent backscatter coefficients (BSCs) computed with the SFM for different aggregate compactnesses and a constant aggregate size $r_{ag}/a = 6.32$ at systemic hematocrits of 10% and 20%, and corresponding fitting with the SFSE (in dashed lines) and with the EMTSFM (in solid lines).

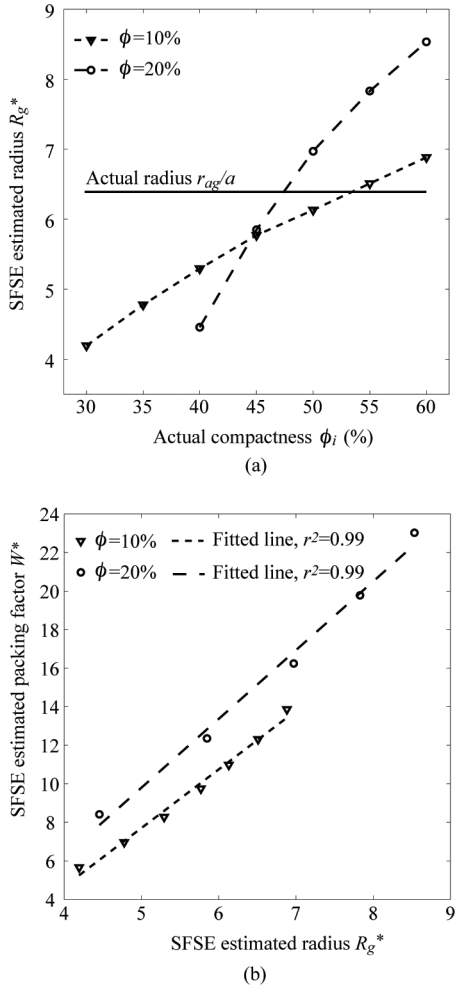

Fig. 4. (a) Aggregate size R_g^* estimated with the SFSE as a function of different aggregate compactnesses for systemic hematocrits of 10% and 20%. The solid line represents the actual aggregate size $r_{ag}/a = 6.32$. (b) Linear relationships between W^* and R_g^*. Results presented here correspond to the configuration where ϕ_i varies and r_{ag}/a is fixed.

systemic hematocrits. Excellent correlations ($r^2 \geq 0.92$) were found between the estimated and true aggregate radii for all hematocrits (data not shown). The estimated values a^*_{eff}/a and ϕ_i^* from the GM and the corresponding relative errors are given in Fig. 8. For systemic hematocrits of 10% and 20%, the estimated radii and compactnesses are quantitatively satisfactory with relative errors less than 15%. However, for $\phi = 30\%$, the relative errors increase to 40%.

For the clustering conditions in which the aggregate compactness varied and the aggregate radius was constant, the results are shown in Fig. 9 for systemic hematocrits of 10% and 20%. As previously observed with the SFSE, the estimated effective radius increases as the aggregate compactness increases. The estimated radii and compactnesses matched the true parameters at $\phi = 10\%$ with relative errors less than 17%. However, for $\phi = 20\%$, large relative errors (up to 74%) were obtained.

4) Comparison of the Errors Between the Simulated BSC and the Fitted Curves With the Three Scattering Models: The errors (i.e., differences) between the simulated BSC and the fitted curves with the three scattering models (SFSE, EMTSFM, and GM) are presented in Fig. 10. The logarithm of the error is shown to enhance readability.

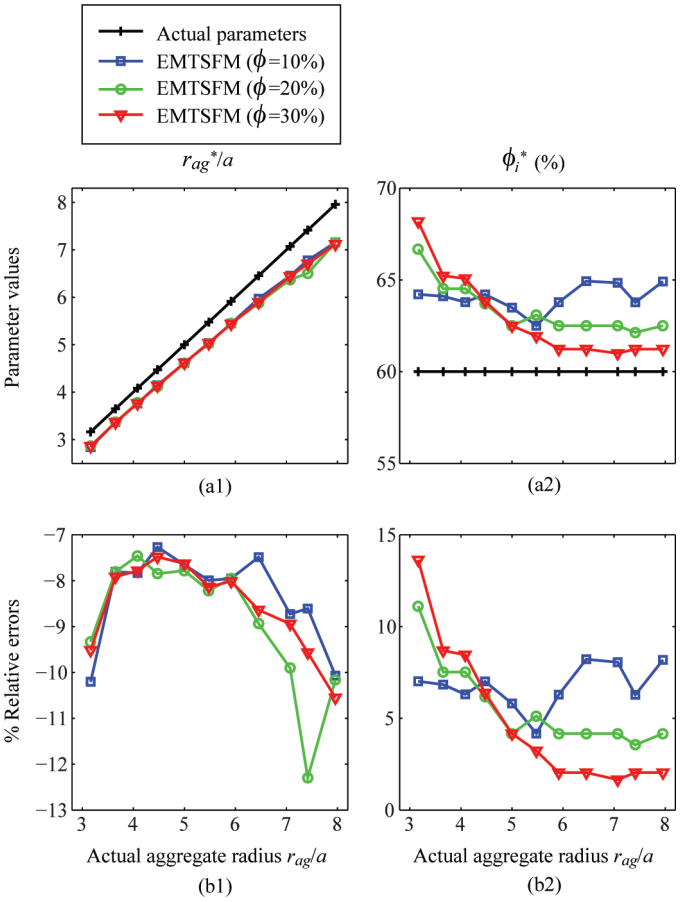

Fig. 5. (a) Values of r^*_{ag}/a and ϕ_i^* estimated by the EMTSFM as a function of the actual aggregate radius for the three systemic hematocrits of 10%, 20%, and 30%. Also represented are actual values of r_{ag}/a and ϕ_i. (b) Corresponding relative errors of r^*_{ag}/a and ϕ_i^*.

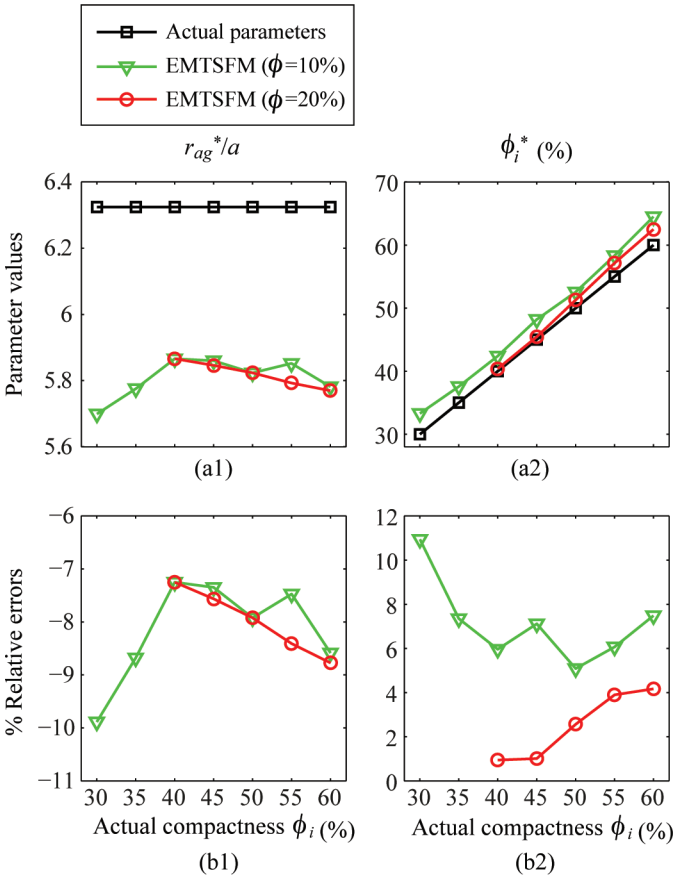

Fig. 6. (a) Values of r^*_{ag}/a and ϕ_i^* estimated by the EMTSFM as a function of the actual aggregate compactness for the systemic hematocrits of 10% and 20%. Also represented are actual values of r_{ag}/a and ϕ_i. (b) Corresponding relative errors of r^*_{ag}/a and ϕ_i^*.

The error reveals how the models fit the data. It is clear from the figure that errors were smaller with the EMTSFM and larger with the GM for each hematocrit. For the aggregating conditions in which the aggregate radius varied, the error decreases as the radius increases. When the aggregate radius increases, the frequency bandwidth used for the fit becomes smaller, and therefore the number of frequencies used for the error computation decreases.

B. Results Obtained From the 3-D Computer Simulations

For the 3-D computer simulations, the GM, SFSE, and EMTSFM were examined when the aggregate size varied and the aggregate compactness was fixed to a high value: $\phi_i = 74\%$.

It is important to note that the 3-D simulated aggregates were highly packed, leaving small numbers of particles as non-aggregated RBCs. For each tissue realization, the actual mean aggregate radius r_{ag} was computed using [11, Eq. (6)], and then the concentration of aggregated RBCs ϕ' was computed as

$$\phi' = \frac{\phi_i N_{\text{ag}} (4/3)\pi r_{\text{ag}}^3}{1000 \times 125 \times 125 \times (10^{-6})^3}. \tag{13}$$

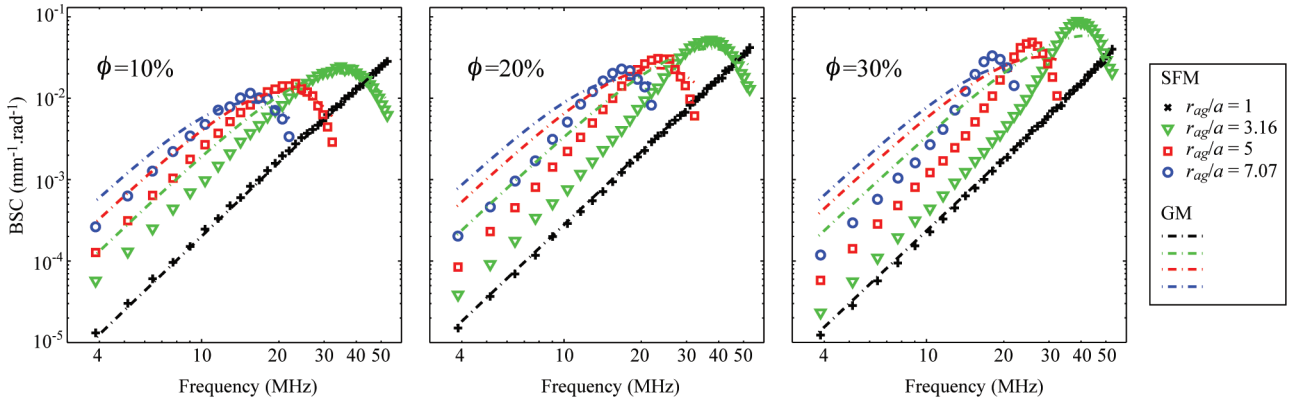

Fig. 7. Frequency-dependent backscatter coefficients (BSCs) computed with the SFM for different aggregate sizes and a constant aggregate compactness $\phi_i = 60\%$ at systemic hematocrits of 10%, 20%, and 30%, and corresponding fitting with the GM.

Fig. 11(a) shows the values of ϕ' as a function of the mean aggregate radius r_{ag}/a for the three systemic hematocrits of 20%, 30%, and 40%. The percentage of disaggregated RBCs was between 20% and 30% for the systemic hematocrit of 20% and between 27% and 37% for the systemic hematocrit of 40%. Note that the three models presented in Section III assumed that all RBCs were aggregated in blood and that aggregates had identical shape and size. Consequently, during the inversion procedure of the 3-D BSC data, we neglected the contribution of the disaggregated RBCs on the simulated $\mathrm{BSC_{SFM}}$ and we replaced the hematocrit ϕ by the value of the concentration of aggregated RBCs ϕ'.

Figs. 11(b) and 11(c) show $\mathrm{BSC_{SFM}}$ as a function of frequency for several aggregate sizes and systemic hematocrits of 30% and 40%. Also represented in Figs. 11(b) and 11(c) are corresponding fitted curves obtained with the SFSE, EMTSFM, and GM. The fitted GM and SFSE

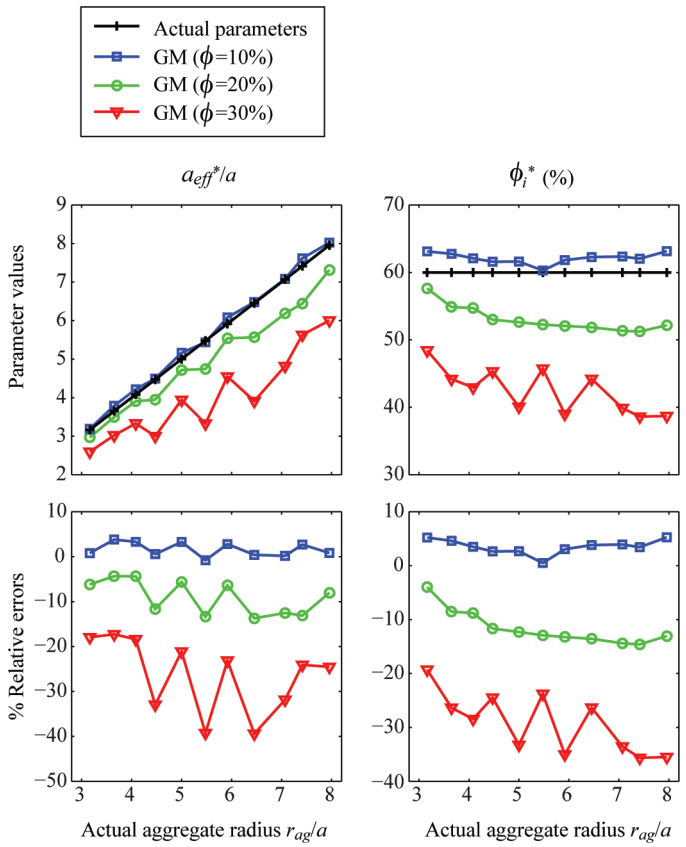

Fig. 8. (Top) Values of a_{eff}^*/a and ϕ_i^* estimated by the GM as a function of the actual aggregate radius for the three systemic hematocrits of 10%, 20%, and 30%. Also represented are actual values of r_{ag}/a and ϕ_i. (Bottom) Corresponding relative errors of a_{eff}^*/a and ϕ_i^*.

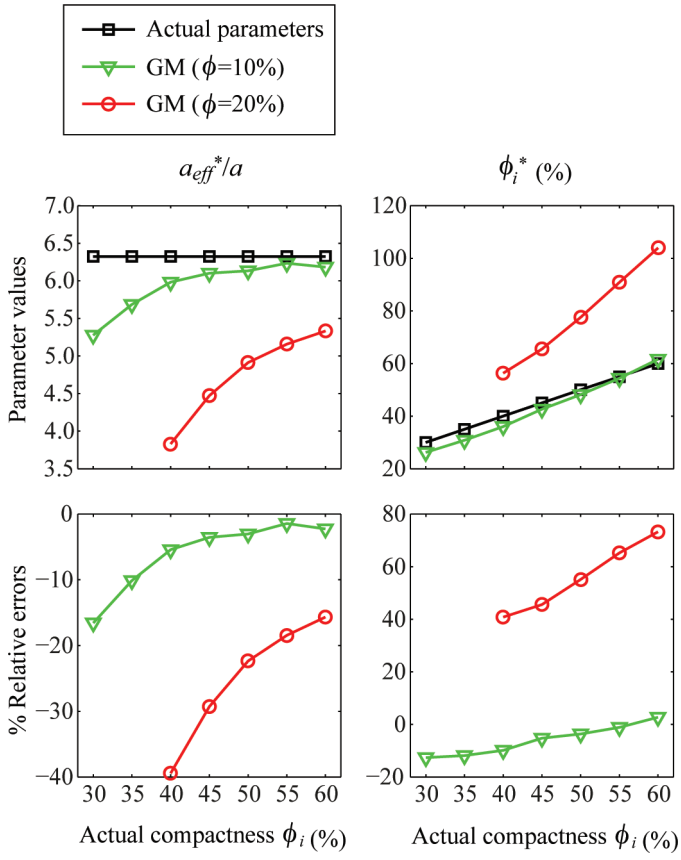

Fig. 9. (Top) Values of a_{eff}^*/a and ϕ_i^* estimated by the GM as a function of the actual aggregate compactness for the systemic hematocrits of 10% and 20%. Also represented are actual values of r_{ag}/a and ϕ_i. (Bottom) Corresponding relative errors of a_{eff}^*/a and ϕ_i^*.

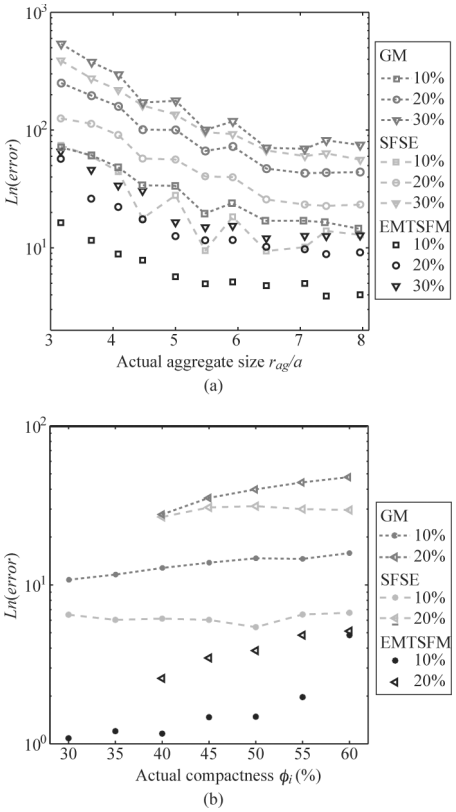

Fig. 10. Logarithm of the error between the simulated BSC_{SFM} and the fitted curves with the three scattering models GM, SFSE, and EMTSFM. (a) As a function of the actual aggregate size for the clustering configuration where r_{ag}/a varies and ϕ_i is fixed. (b) As a function of the actual aggregate compactness for the clustering configuration where ϕ_i varies and r_{ag}/a is fixed.

curves did not produce good fits to the 3-D data and overestimated the BSC_{SFM} amplitude (especially in the low frequency range), as observed in the 2-D case (see Figs. 1 and 7). On the contrary, the EMTSFM provided good fittings to the simulated BSC_{SFM} curves.

The results obtained with the SFSE were already presented in a previous article [11]. Excellent correlations ($r^2 \geq 0.94$) were found between the estimated and true aggregate radii for all hematocrits (see [11, Fig. 5(a)]). It can also be seen in [11, Fig. 5(a)] that for each hematocrit there is an aggregate size range for which the SFSE method works at its best. For example, relative errors for estimated radii were less than 20% for true radius values between 14 and 17 μm at the hematocrit of 40%. The parameters W^* and R^*_{sp} followed a quadratic relationship (as in [11, Fig. 5(b)]).

Fig. 12 gives the values of r^*_{ag} and ϕ^*_i estimated with the EMTSFM and corresponding relative errors that were less than 15% and 23%, respectively, for all hematocrits. Fig. 13 gives the values of a^*_{eff} and ϕ^*_i estimated with the GM and corresponding relative errors. The estimated radii with the new formulation of the GM are quantitatively satisfactory, with relative errors less than 9% for all hematocrits. The relative errors for the estimated compactnesses with the GM are larger with relative errors up to 32% for the hematocrits of 20% and 30%, and up to 76% for the hematocrit of 40%.

V. Discussion and Conclusions

Three scattering models for the characterization of RBC aggregation were examined. From these models, the gold-standard simulated BSC_{SFM} was fitted and aggregation parameters were extracted. The SFSE has been developed for blood characterization and the GM is a model that has been used in various tissue studies. Herein, the radius estimates R_g from the SFSE and a_{eff} from the GM were hypothesized to represent the aggregate size.

A. Clustering Conditions in Which the Aggregate Radius Varied and the Aggregate Compactness Was Constant (2-D and 3-D Computer Simulations)

The 2-D and 3-D computer simulations were performed on the same clustering configuration in which the aggre-

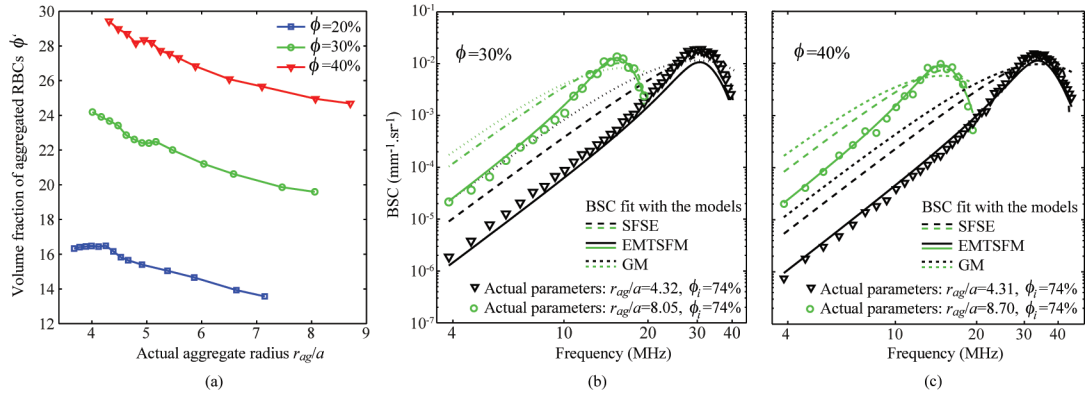

Fig. 11. (a) Concentration of aggregated red blood cells (RBCs) ϕ' as a function of the mean aggregate radius r_{ag}/a for the three systemic hematocrits of 20%, 30%, and 40%. (b) and (c) Frequency-dependent backscatter coefficients (BSCs) computed with the SFM in the 3-D case for different aggregate sizes and a constant aggregate compactness $\phi_i = 74\%$ at systemic hematocrits of 30% and 40%, and corresponding fitting with the SFSE model, the EMTSFM, and the GM.

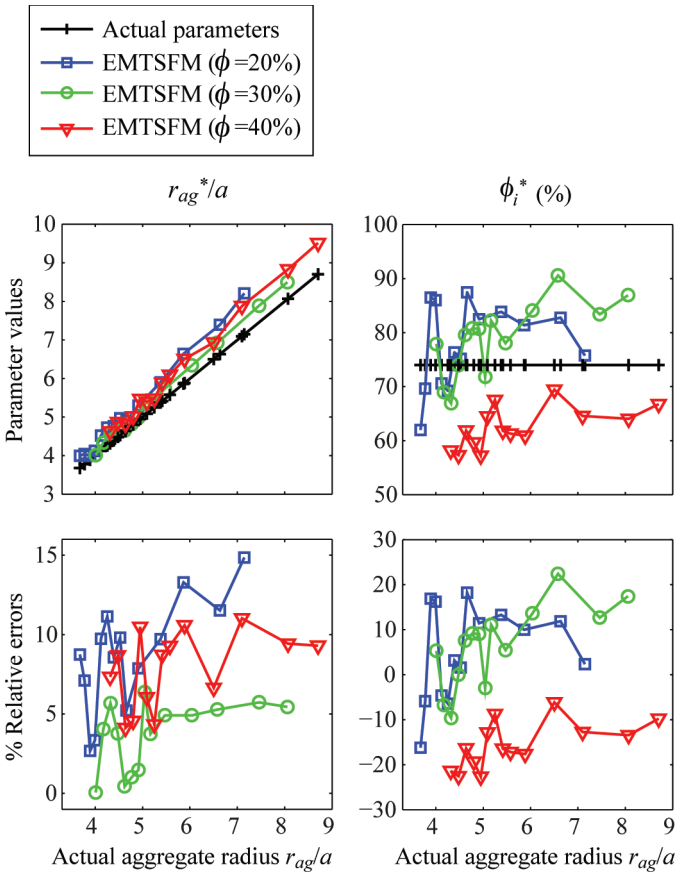

Fig. 12. (Top) Values of r_{ag}^*/a and ϕ_i^* estimated by the EMTSFM as a function of the actual aggregate radius for the three systemic hematocrits of 20%, 30%, and 40%. Also represented are actual values of r_{ag}/a and ϕ_i. (Bottom) Corresponding relative errors of r_{ag}^*/a and ϕ_i^*.

gate radius varied and the aggregate compactness was constant. It is interesting to observe the same BSC_{SFM} behavior for both 2-D and 3-D studies. Indeed, the simulated BSC_{SFM} amplitude increases with the size of aggregates and the BSC_{SFM} first peaks occur at lower frequencies as the aggregate radius increases (see Fig. 1 in the 2-D case, and Figs. 11(b) and 11(c) and [11, Fig. 4] in the 3-D case). Moreover, as can be observed in Figs. 1 and 7 in the 2-D case and in Fig. 11 in the 3-D case, the data fitting qualities obtained with the three models were quite similar. In both 2-D and 3-D cases, it is clear that the GM and the SFSE are insufficient to model the complex behavior of BSC and that the EMTSFM was the model that better fitted the BSC data for all studied hematocrits.

Although the SFSE model did not produce good spectral fits to the BSC data for 2-D and 3-D computer simulations, significant correlations were found between the estimated and true radii with r^2 superior to 0.95 at all hematocrits (see Fig. 2(a) and [11, Fig. 5(a)]). However, the estimated aggregation parameters W^* and R_g^* followed a linear relationship in our 2-D simulation study. This relation was also found to be quadratic in 3-D numerical simulations [11] and under experimental conditions [10]. It means that the BSC parameterization can be reduced to one parameter and that no new information can be obtained with the parameter W^*.

The EMTSFM and the GM used as effective medium models gave quantitatively satisfactory radius estimates with relative errors less than 15% for the 10% and 20% hematocrits in the 2-D case, and for all hematocrits in the 3-D case. For the highest systemic hematocrit, the aggregate compactnesses were better estimated with the EMTSFM, with relative errors less than 14% in the 2-D case (and less than 23% in the 3-D case), whereas the relative errors were between 19% and 36% in the 2-D case (and between 59% and 76% in the 3-D case) for the GM. These results with the EMTSFM and the GM were somewhat anticipated because the assumption of a random distribution of scatterers used by the GM fails because of the spatial correlation between scatterers in a dense medium [24]. To conclude, the EMTSFM was more suitable than the GM and SFSE for characterizing the aggregate microstructure in both 2-D and 3-D studies.

B. Clustering Conditions in Which the Aggregate Compactness Varied and the Aggregate Radius Was Constant (2-D Computer Simulations)

For the highest simulated hematocrit of 20%, the aggregate radii normalized by the RBC radius were estimated between 4.34 and 8.55 using the SFSE model and between 3.83 and 5.33 using the GM (see Figs. 4(a) and 9), whereas the actual aggregate radius was $r_{ag}/a = 6.32$. Therefore, we found no correlation between the actual fixed aggregate radius and the estimated radii. The GM and SFSE cannot take into account a variation in the aggregate compactness at a large hematocrit, because it is interpreted as a change in the aggregate size.

In the case of the SFSE, one could have expected a fixed value of the estimated radius R_g^* and a variation of the estimated packing factor W^*, when the aggregate radius was fixed and the aggregate compactness varied. However, both R_g^* and W^* increased as the true aggregate compactness was raised. The estimated parameters R_g^* and W^* followed linear relations for all hematocrits [see Fig. 4(b)], as observed previously in Fig. 2(b) when the aggregate radius r_{ag}/a was changed. It means that W^* and R_g^* carry the same information and that the BSC parameterization is reduced to one parameter.

The estimated parameters using the EMTSFM presented in Fig. 6 show that the model gave quantitatively satisfactory estimates for all aggregate compactnesses and for all studied hematocrits. Contrary to the GM and SFSE, the EMTSFM provided a quasi-constant aggregate radii between 5.7 and 5.9 for both studied hematocrits. Moreover, the aggregate compactnesses were estimated with relative errors less than 12% at both studied hematocrits for that model. The errors between simulated BSC_{SFM} and the fitted curves were also smaller with the EMTSFM, as can be observed in Fig. 10(b). To conclude, the EMTS-

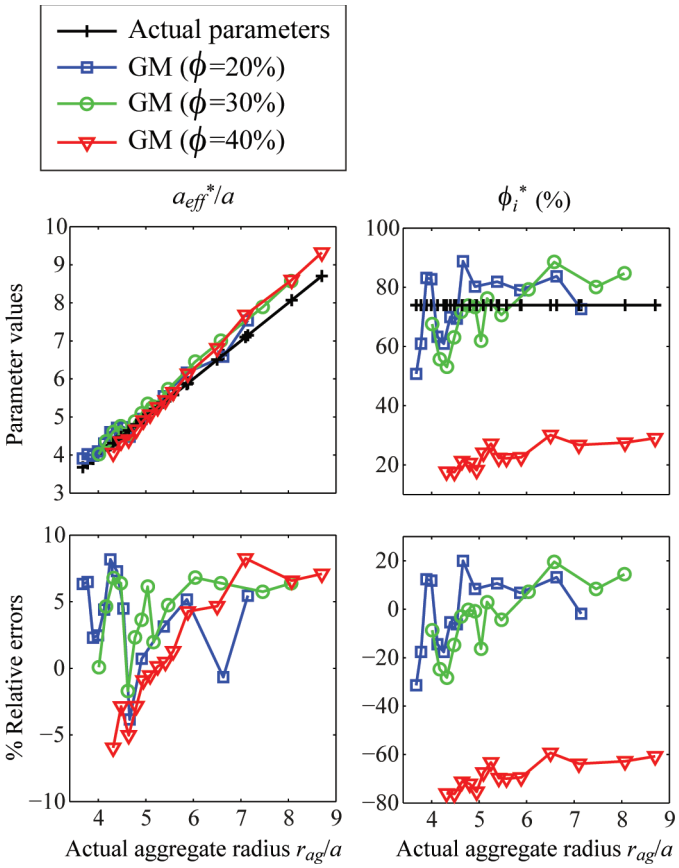

Fig. 13. (Top) Values of a_{eff}^*/a and ϕ_i^* estimated by the GM as a function of the actual aggregate radius for the three systemic hematocrits of 20%, 30%, and 40%. Also represented are actual values of r_{ag}/a and ϕ_i. (Bottom) Corresponding relative errors of a_{eff}^*/a and ϕ_i^*.

FM was the model that better explained the simulated BSC_{SFM}.

C. Computation of RBC Distributions and of BSC_{SFM}

The two methods we used here to obtain the RBC spatial distributions did not take into consideration realistic interactions between RBCs. These methods were already presented in [12] and [11] for the 2-D and 3-D computer simulations, respectively. They were simple and fast methods to generate samples containing non-overlapping, identical and isotropic aggregates. The 3-D computer simulations allowed better mimicking of real data but they are time consuming (see [11, Sections III-A and V] to obtain a quick review of different approaches for simulating compact RBC aggregates). To simulate the BSC data with the SFM reference model, the method we chose to distribute RBCs in the 3-D case allowed 1) studying of various aggregate sizes with the same aggregate compactness and 2) reaching the physiological hematocrit of 40% by mixing identical RBC aggregates and disaggregated RBCs. Because studied scattering models assumed that all RBCs were aggregated in blood and because the average percentage of disaggregated RBCs was small (around 25%), the influence of the disaggregated RBCs on the simulated BSC_{SFM} was neglected during the inversion procedure of the 3-D BSC data. Contrary to the 3-D modeling, the method we chose to distribute RBCs in the 2-D case allowed 1) studying of the clustering condition in which the aggregate compactness varies and the aggregate size is fixed and 2) having only aggregated RBCs in blood. However, the 2-D computer simulations were limited to a maximum hematocrit of 30% because of the difficulty to simulate with the SFM values greater than 30%. To clarify, the main difficulty in the 2-D case was to distribute compact aggregates and to have only aggregated RBCs in blood. The maximum value of the aggregate area fraction $\phi_{\text{ag}_{\max}}$ was fixed to 0.5, corresponding to the maximum particle area fraction that can be easily generated using a random number generator. The procedure we chose to distribute the RBCs within aggregates allows reaching a maximum value of aggregate compactness $\phi_{i_{\max}}$ equal to 0.6 (see [12, Section III-B]). As a consequence, the maximum value of the systemic hematocrit was limited to $\phi_{\max} = \phi_{\text{ag}_{\max}}\phi_{i_{\max}} = 0.3$.

We also modeled individual biconcave RBCs as spheres of equivalent volume in the 3-D study and studied BSC between 4 and 45 MHz. The impact of modeling a RBC by a sphere on the frequency dependence of the backscatter cross section has been studied and errors are introduced above 20 MHz [16], [25]. The impact of this simplification on the simulated BSC_{SFM} and structural aggregate estimates with the three models (SFSE, GM, and EMTSFM) is unknown and still needs to be explored.

D. On the Use of the EMTSFM In Vivo

The EMTSFM assumes that all RBCs are aggregated in blood and that aggregates are identical and isotropic. Therefore, the BSC behavior obtained in our simulations has pronounced frequency peaks. In experimental conditions [10], the BSC behavior was smoother and the peaks were less pronounced. The reason behind this might be that real blood contains several sizes of aggregates and, because the location of BSC peaks are different for different aggregate populations, a relatively smoother BSC curve can be obtained. Another important aspect to consider is the assumption of isotropic aggregates. In human blood, low shear rates can promote the formation of RBC aggregates having anisotropic (i.e., rouleaux) or isotropic (i.e., clump) structures. The rouleaux-like pattern is typically associated with normal blood. However, as the binding energy between RBCs increases with inflammation [26], aggregates form clump structures, as in diabetes mellitus [14], [15]. The assumption of isotropic aggregates in the EMTSFM is thus valid as far as we are concerned with the study of pathological states. In the case of normal human rouleaux of RBCs, if the EMTSFM is applied to estimate structural parameters such as the aggregate size and compactness, this assumption would obviously create a bias against the parameter estimation. Therefore, future improvements should consider incorporating

the aggregate anisotropy and the polydispersity in terms of aggregate size and compactness to provide an optimal model for the inversion of experimental data. Future validations may also evaluate the EMTSFM in a controlled Couette flow experiment with ghost RBCs (i.e., optically visible RBCs with no hemoglobin and viable membrane properties) coated with dextran polymers to change attractive energies between erythrocytes and thus modulate the aggregate compactness and size.

Another difficulty in applying the EMTSFM *in vivo* is that the spectral content of backscattered echoes is also affected by attenuation caused by intervening tissue layers (such as the skin) between the probe and the blood flow. To correctly evaluate microstructural parameters, it is thus of major interest to take into account tissue attenuation effects. Note that the SFSE was slightly modified to introduce the attenuation term in the BSC expression and was named the structure factor size and attenuation estimator (SFSAE) [27]. The SFSAE allows to determine simultaneously blood structural parameters (i.e., W^* and R_g^*) and the total attenuation [28], [29]. Future improvements of the EMTSFM should incorporate the tissue attenuation as for the SFSAE. This means that the EMTSFM should be slightly modified by introducing the attenuation term to simultaneously estimate the RBC aggregate size, compactness, and the total attenuation.

Appendix A
Numerical Computation of the Structure Factor S_{AG} for Hard Cylinders in 2-D

Because there is no analytical expression of the structure factor S_{ag} for hard cylinders in 2-D [30], [31], S_{ag} was numerically computed for several values of ϕ_{ag} varying from 0.01 to 0.5 with a step of 0.01. This means that, in the 2-D case, the cylinder concentration ϕ_{ag} was rounded to the second decimal for the computation of S_{ag} in (7). Note that the computation of S_{ag} depends not only on the area fraction ϕ_{ag} but also on the effective particle radius r_{ag}. That is why S_{ag} that depends on r_{ag} was computed in a dimensionless way as described next.

For each specified value of ϕ_{ag}, aggregates of an arbitrarily normalized (dimensionless) radius of 1/60 were randomly distributed within a dimensionless surface area $L'^2 = 1 \times 1$ with non-overlapping positions using a random number generator. The corresponding density matrix D' was computed by dividing the square simulation plane L'^2 into N_{p}^2 pixels (herein, $N_{\mathrm{p}} = 512$) and by counting the number of particles falling into each pixel. The Fourier transformation of the density matrix D' was then computed to generate a structure factor S_{ag}. A mean S_{ag} was determined by repeating this procedure 400 times. When the value of the effective particle radius r_{ag} was specified, the centered grid of wavevectors for the structure factor S_{ag} was computed between $\pm(\pi N_p)/(2 \times 60 r_{\mathrm{ag}})$ with a step of $\Delta k = \pi/60 r_{\mathrm{ag}}$ (i.e., by putting the simulated surface length $L' = 60 r_{\mathrm{ag}}$).

Appendix B
Analytical Expression of the Structure Factor S_{AG} For Hard Spheres in 3-D

The structure factor S for hard spheres is given by [23], [32]

$$S(k) = \frac{1}{1 - 4\pi m d^3 \int_0^1 z^2 \frac{\sin(2kz)}{2kz} c(z) \mathrm{d}z}, \tag{14}$$

where m is the number density of hard spheres, d is the hard sphere diameter, and $c(z)$ is the direct correlation function given by [23], [32]

$$-c(z) = \begin{cases} c_0 + c_1 \dfrac{z}{d} + c_3 \left(\dfrac{z}{d}\right)^3 & \text{for } z \le d \\ 0 & \text{for } z > d. \end{cases} \tag{15}$$

The coefficients c_0, c_1, and c_3 are given by [23], [32]

$$\begin{aligned} c_0 &= \frac{(1+2\phi)^2}{(1-\phi)^4} \\ c_1 &= -\frac{6\phi(1+\phi/2)^2}{(1-\phi)^4} \\ c_2 &= \frac{\phi}{2} c_0 = \frac{\phi(1+2\phi)^2}{2(1-\phi)^4}. \end{aligned} \tag{16}$$

References

[1] F. L. Lizzi, M. Ostromogilsky, E. J. Feleppa, M. C. Rorke, and M. M. Yaremko, "Relationship of ultrasonic spectral parameters to features of tissue microstructure," *IEEE Trans. Ultrason. Ferroelectr. Freq. Control*, vol. 34, no. 3, pp. 319–329, 1987.

[2] M. F. Insana, R. F. Wagner, D. G. Brown, and T. J. Hall, "Describing small-scale structure in random media using pulse-echo ultrasound," *J. Acoust. Soc. Am.*, vol. 87, no. 1, pp. 179–192, 1990.

[3] E. J. Feleppa, F. L. Lizzi, D. J. Coleman, and M. M. Yaremko, "Diagnostic spectrum analysis in ophthalmology: A physical perspective," *Ultrasound Med. Biol.*, vol. 12, no. 8, pp. 623–631, 1986.

[4] E. J. Feleppa, T. Liu, A. Kalisz, M. C. Shao, N. Fleshner, and V. Reuter, "Ultrasonic spectral-parameter imaging of the prostate," *Int. J. Imaging Syst. Technol.*, vol. 8, no. 1, pp. 11–25, 1997.

[5] M. L. Oelze, W. D. O'Brien, J. P. Blue, and J. F. Zachary, "Differentiation and characterization of rat mammary fibroadenomas and 4T1 mouse carcinomas using quantitative ultrasound imaging," *IEEE Trans. Med. Imaging*, vol. 23, no. 6, pp. 764–771, 2004.

[6] H. Kitamura, B. Sigel, J. Machi, E. J. Feleppa, J. Sokil-Melgar, and J. Justin, "Roles of hematocrit and fibrinogen in red cell aggregation determined by ultrasonic scattering properties," *Ultrasound Med. Biol.*, vol. 21, no. 6, pp. 827–832, 1995.

[7] R. B. Ami, G. Barshtein, D. Zeltser, Y. Goldberg, I. Shapira, A. Roth, G. Keren, H. Miller, V. Prochorov, A. Eldor, S. Berliner, and S. Yedgar, "Parameters of red blood cell aggregation as correlates of the inflammatory state," *Am. J. Physiol. Heart Circ. Physiol.*, vol. 280, no. 5, pp. H1982–H1988, 2001.

[8] D. Savery and G. Cloutier, "A point process approach to assess the frequency dependence of ultrasound backscattering by aggregating red blood cells," *J. Acoust. Soc. Am.*, vol. 110, no. 6, pp. 3252–3262, 2001.

[9] I. Fontaine, D. Savery, and G. Cloutier, "Simulation of ultrasound backscattering by red blood cell aggregates: Effect of shear rate and anisotropy," *Biophys. J.*, vol. 82, no. 4, pp. 1696–1710, 2002.

[10] F. T. H. Yu and G. Cloutier, "Experimental ultrasound characterization of red blood cell aggregation using the structure factor size estimator," *J. Acoust. Soc. Am.*, vol. 122, no. 1, pp. 645–656, 2007.
[11] R. K. Saha, E. Franceschini, and G. Cloutier, "Assessment of accuracy of the structure-factor-size-estimator method in determining red blood cell aggregate size from ultrasound spectrum backscattering coefficient," *J. Acoust. Soc. Am.*, vol. 129, no. 4, pp. 2269–2277, 2011.
[12] E. Franceschini, B. Metzger, and G. Cloutier, "Forward problem study of an effective medium model for ultrasound blood characterization," *IEEE Trans. Ultrason. Ferroelectr. Freq. Control*, vol. 58, no. 12, pp. 2668–2679, 2011.
[13] O. K. Baskurt, M. R. Hardeman, M. W. Rampling and H. J. Meiselman, Eds., *Handbook of Hemorheology and Hemodynamics*, Washington, DC: IOS Press, 2007.
[14] H. Schmid-Schonbein, H. Malotta, and F. Striesow, "Erythrocyte aggregation: Causes, consequences, and methods of assessment," *Tijdschr NVKS*, vol. 15, pp. 88–97, 1990.
[15] H. Schmid-Schonbein, G. Gallasch, J. V. Gosen, E. Volger, and H. J. Klose, "Red cell aggregation in blood flow. I. New methods of quantification," *Klin. Wochenschr.*, vol. 54, no. 4, pp. 149–157, 1976.
[16] D. Savery and G. Cloutier, "High-frequency ultrasound backscattering by blood: Analytical and semi-analytical models of the erythrocyte cross section," *J. Acoust. Soc. Am.*, vol. 23, no. 4, pp. 3963–3971, 2007.
[17] P. M. Morse and K. U. Ingard, *Theoretical Acoustics*. Princeton, NJ: Princeton University Press, 1968, ch. 8, pp. 400–466.
[18] M. F. Insana and D. G. Brown, "Acoustic scattering theory applied to soft biological tissues," in *Ultrasonic Scattering in Biological Tissues*, K. K. Shung and G. A. Thieme, Eds., Boca Raton, FL: CRC Press, 1993, ch. 4, pp. 76–124.
[19] I. Fontaine, M. Bertrand, and G. Cloutier, "A system-based approach to modeling the ultrasound signal backscattered by red blood cells," *Biophys. J.*, vol. 77, no. 5, pp. 2387–2399, 1999.
[20] V. Twersky, "Low-frequency scattering by correlated distributions of randomly oriented particles," *J. Acoust. Soc. Am.*, vol. 81, no. 5, pp. 1609–1618, 1987.
[21] K. K. Shung, "On the ultrasound scattering from blood as a function of hematocrit," *IEEE Trans. Sonics Ultrason.*, vol. SU-29, no. 6, pp. 327–331, 1982.
[22] A. Guinier and J. Fournet, *Small Angle Scattering of X-Rays*. New York, NY: Wiley Interscience, 1955, ch. 14, pp. 637–669.
[23] M. S. Wertheim, "Exact solution of the Percus–Yevick integral equation for hard spheres," *Phys. Rev. Lett.*, vol. 10, no. 8, pp. 321–323, 1963.
[24] E. Franceschini and R. Guillermin, "Experimental assessment of four ultrasound scattering models for characterizing concentrated tissue-mimicking phantoms," *J. Acoust. Soc. Am.*, vol. 132, no. 6, pp. 3735–3747, 2012.
[25] C. C. Coussios, "The significance of shape and orientation in single-particle weak-scatterer models," *J. Acoust. Soc. Am.*, vol. 112, no. 3, pt. 1, pp. 906–915, 2002.
[26] X. Weng, G. Cloutier, R. Beaulieu, and G. O. Roederer, "Influence of acute-phase proteins on erythrocyte aggregation," *Am. J. Physiol.*, vol. 271, no. 6, pt. 2, pp. H2346–H2352, 1996.
[27] E. Franceschini, F. T. H. Yu, F. Destrempes, and G. Cloutier, "Ultrasound characterization of red blood cell aggregation with intervening attenuating tissue-mimicking phantoms," *J. Acoust. Soc. Am.*, vol. 127, no. 2, pp. 1104–1115, 2010.
[28] F. T. H. Yu, J. K. Armstrong, J. Tripette, H. J. Meiselman, and G. Cloutier, "A local increase in red blood cell aggregation can trigger deep vein thrombosis: Evidence based on quantitative cellular ultrasound imaging," *J. Thromb. Haemost.*, vol. 9, no. 3, pp. 481–488, 2011.
[29] J. Tripette, A. Y. Denault, L. Allard, B. Chayer, L. P. Perrault, and G. Cloutier, "Ultrasound monitoring of RBC aggregation as a real-time marker of the inflammatory response in a cardiopulmonary bypass swine model," *Crit. Care Med.*, vol. 41, no. 8, pp. e171–e178, 2013.
[30] C. F. Tejero and J. A. Cuesta, "Hard-sphere and hard-disk freezing from the differential formulation of the generalized effective liquid approximation," *Phys. Rev. E*, vol. 47, no. 1, pp. 490–495, 1993.
[31] X. Guo and U. Riebel, "Theoretical direct correlation function for two-dimensional fluids of monodisperse hard spheres," *J. Chem. Phys.*, vol. 125, no. 14, art. no. 144504, 2006.
[32] N. W. Ashcroft, "Structure and resistivity of liquid metals," *Phys. Rev.*, vol. 145, no. 1, pp. 83–90, 1966.

Emilie Franceschini received her M.S. degree in mechanical engineering from the Ecole Supérieure d'Ingénieurs de Marseille in 2003, and the Ph.D. degree in acoustics from the University of Provence, Marseille, in 2006. In 2007, she was a Postdoctoral Fellow at the Laboratory of Biorheology and Medical Ultrasonics, Research Center of the University of Montreal Hospital, Montreal, QC. Since October 2008, she has been a Researcher at the French National Centre for Scientific Research (CNRS) in the Laboratory of Mechanics and Acoustics CNRS UPR 7051, Marseille. Her current research interests include ultrasound imaging for biomedical applications, inverse problems, and ultrasound characterization of biological tissues at the microscopic level. She is a member of the French Acoustical Society (SFA) and IEEE.

Ratan K. Saha obtained his B.Sc. degree in physics (studied at A.B.N. Seal College, Coochbehar, India) from the University of North Bengal, Siliguri, India, in 1996 and received his M.Sc. degree in physics from Jadavpur University, Kolkata, India, in 1999. He carried out his Ph.D. work at the Saha Institute of Nuclear Physics, Kolkata from 2000 to 2006. He then joined the Laboratory of Biorheology and Medical Ultrasonics, Research Center of the University of Montreal Hospital, Montreal, Canada, as a postdoctoral fellow from 2007 to 2008. He also worked as a postdoctoral fellow at Ryerson University, Toronto, Canada, from 2009 to 2011. Since October 2011, he has been a postdoctoral fellow at the Saha Institute of Nuclear Physics and his current research interests include ultrasonic and photoacoustic characterizations of soft tissues.

Guy Cloutier (S'89–M'90–SM'07) obtained his B.Eng. degree in electrical engineering in 1984, and his M.Sc. and Ph.D. degrees in biomedical engineering in 1986 and 1990, respectively. Between 1990 and 1992, he was a postdoctoral fellow at The Pennsylvania State University with Prof. K. Kirk Shung. Prof. Cloutier is Director of the Laboratory of Biorheology and Medical Ultrasonics at the University of Montreal Hospital Research Center (www.lbum-crchum.com), and Professor of Radiology and Biomedical Engineering at the University of Montreal. His research interests are in quantitative ultrasound imaging of red blood cell aggregation, quasi-static and dynamic ultrasound elastography of atherosclerotic plaques, vascular aneurysms, deep vein thrombi and breast cancers, 3-D morphologic and hemodynamic assessment of lower limb arterial stenoses, and mathematical and biomechanical modeling. He has published more than 140 peer-reviewed articles in these fields, holds 11 patents, and was recipient of the National Scientist award of the Fonds de Recherche en Santé du Québec (2004 to 2009).